Water Air Soil Pollut (2020) 231: 163
https://doi.org/10.1007/s11270-020-04535-9

Synthesis and Characterization of Chitosan/Fluorapatite Composites for the Removal of Cr (VI) from Aqueous Solutions and Optimized Parameters

Rachid El Kaim Billah · Youness Abdellaoui · Zakaria Anfar · Germán Giácoman-Vallejos · Mahfoud Agunaou · Abdessadik Soufiane

Received: 6 December 2019 / Accepted: 13 March 2020 / Published online: 31 March 2020

Abstract In the present work, chitosan/fluorapatite composite was successfully prepared and applied for the removal of chromium (VI). The synthesized materials were characterized using X-rays diffraction (XRD), Fourier-transform infrared spectroscopy (FTIR), scanning electronic microscopy (SEM), and energy-dispersive X-ray spectroscopy (EDS). The thermogravimetric analysis (TGA) and pH of the point of zero charge (pH_{PZC}) were also considered as a part of these characterizations. A batch system was carried out to evaluate the effects of contact time, initial Cr (VI) concentration, initial pH, and adsorbent dosage on the adsorption process. The regression coefficient value showed that the experimental data best fit to pseudo-second-order model (PSO), while the Langmuir adsorption isotherms best described the equilibrium adsorption data with highest q_m of 81.34 and 100.92 mg/g for CS and CS-Fa, respectively. Finally, CS-Fa was successfully reused for more than 6 cycles without severe loss in its sorption capacity. The effect of various parameters such as pH, mass, temperature, and contact time was studied using response surface methodology (RSM) and the suggested optimized values by RSM were found to be 2.54 for pH, 25.75 °C, 36.63 min, and 86.72 mg of CS-Fa adsorbent. The maximum adsorption removal efficiency of Cr (VI) was equal to 91.28% under optimum conditions.

Keywords Fluorapatite · Chitosan · Composite · Chromium (VI) removal

Electronic supplementary material The online version of this article (https://doi.org/10.1007/s11270-020-04535-9) contains supplementary material, which is available to authorized users.

R. E. K. Billah · M. Agunaou · A. Soufiane
Department of Chemistry, Faculty of Sciences, Laboratory of Coordination and Analytical Chemistry, University of Chouaib Doukkali, Avenue Jabran Khalil Jabran, B.P 299, 24000 El Jadida, Morocco

Y. Abdellaoui (✉) · G. Giácoman-Vallejos
Facultad de Ingeniería, Universidad Autónoma de Yucatán, Av. Industrias no Contaminantes por Periférico Norte, Cordemex, 150, Mérida, YUC, Mexico
e-mail: abdellaoui.youness@gmail.com

Z. Anfar
Materials and environment laboratory, Ibn Zohr University, 80000 Agadir, Morocco

1 Introduction

Water quality, throughout history, has been an essential factor in ensuring human well-being. Nowadays, one of the most severe environmental problems is the pollution of the hydrosphere, which is to a great extent, threatened by human activity (Streimikiene 2015). The quality of this vital element is deteriorating due to industrial wastes, especially by heavy metals, which are a characteristic feature of these industries and become more and more worrying. The protection of the environment requires the early elimination of these metals, considering the levels allowed by international chemical standards discharged into the wild (Abdellaoui et al. 2019).

The carcinogenic and teratogenic properties on humans of most heavy metals have considered them a severe danger to human beings (Elouahli et al. 2018; Wu et al. 2008). However, chromium can be released into the environment by various industries, including the metal finishing industry, the iron and steel industry, and the production of inorganic chemicals.

The toxicity of chromium depends not only on its concentration but also on its degree of oxidation. Indeed, it is commonly accepted that chromium (VI) is much more toxic than chromium (III). Chromium (VI) ions are a kind of toxic inorganic pollutant that poses a severe problem to ecosystems, whether its effluents are not appropriately treated (Huang et al. 2013).

Among the developed viable technologies for the removal of heavy metals from wastewater effluents is the sorption process as a promising and highly effective method (Cimá-Mukul et al. 2019). Unfortunately, most conventional adsorption systems are broadly applied the activated carbon to remove a variety of contaminants despite its disadvantages relating to the cost of production, separation difficulties, and regeneration (Abatal et al. 2018). Therefore, the researches towards treatment processes using less costly and widely available natural materials are encouraged. Indeed, the performance and effectiveness of this technique depend in a preponderant way of the support nature used as an adsorbent, its cost, abundance, and regeneration.

Recently, research has focused on the study of chitinous products and their derivatives, especially chitosan, owing to its intrinsic properties, abundance, and biodegradability that constitute significant assets for its use for a respective environmental clean-up (Pal and Pal 2019; Sessarego et al. 2019). Moreover, natural minerals showed to be a promising sorbent of heavy metals owing to their excellent environmental compatibility and removal capability, for instance, clay minerals and iron ore slimes (Panda et al. 2011; Uddin 2017). Among these minerals, phosphate rocks exist widely in nature under several mineralogical classes. However, the apatite is considered as the most abundant phosphate on earth (Hughes and Rakovan 2002). Fluorapatite (Fa) with the formula $[Ca_5(PO_4)_3F]$ is one of the most common apatite phases in nature. Natural phosphate showed great potential to be one of the efficient adsorbents (Aklil et al. 2004). Previous works have evaluated the maximum sorption capacity (q_m) of natural phosphate of divalent heavy metals; the q_m was to be 89.29, 32.15, and 23.70 mg/g for Pb (II), Cu (II), and Zn (II), respectively.

Further work demonstrated that modification of natural phosphate with hydroxyl function improves the adsorption capability of heavy metals ions (Mobasherpour et al. 2011; Sun et al. 2018). Furthermore, such as functional groups that strongly react with heavy metals, the importance of amino groups could not be ignored. Therefore, the presence of both amino and hydroxyl groups on chitosan surface made it one of the most prevalent modifier agents, and it has a high affinity for chromium ions and thus could effectively improve the adsorption of Cr (VI) (Aydin and Aksoy 2009; Rojas et al. 2005; Sampaio et al. 2015).

In this context, the work is devoted to the synthesis, characterization of chitosan-fluorapatite (CS-Fa) composite; somehow, it could control and promote the active sites of the CS surface, and then condition the properties of the suitable adsorbent for chromium (VI) ions. Furthermore, an investigation of the different parameters on the sorption of chromium ions using response surface methodology (RSM) and regeneration study of CS-Fa will also be carried out.

2 Materials and Methods

2.1 Materials

Potassium dichromate ($K_2Cr_2O_7$, Sigma-Aldrich, ≥ 99.5%), sodium hydroxide (NaOH, Sigma-Aldrich, ≥ 99%), 1,5-diphenylcarbazide ($C_{13}H_{14}N_4O$, Sigma-Aldrich, ≥ 98%), nitric acid (HNO_3, Sigma-Aldrich, 65%), hydrochloric acid (HCl, Sigma-Aldrich, 37%), sulfuric acid (H_2SO_4, Sigma-Aldrich, 37%), ethanol (C_2H_5OH, Sigma-Aldrich, ≥ 95%) are applied. The CAS registry number, mass fraction

purity, and supplies' name of all chemicals are listed in Table 1.

2.2 Adsorbent Preparation

2.2.1 Preparation of Chitosan

Crude chitin was extracted from shrimp shells, which was then processed to obtain chitosan (CS). CS was obtained using chemical deacetylation process where the chitin was brought in contact with a solution of sodium hydroxide NaOH (48 wt%) at a temperature of 100 °C, for 6 h with a solid-to-liquid ratio of 1:20 to remove some or all the acetyl groups of the chitin. The product obtained was then filtered and washed several times with distilled water until neutral pH was reached, the substrate was dried at $T = 50$ °C. The obtained chitosan was labeled as CS.

2.2.2 Preparation of Fluorapatite

The natural phosphate used in the present work comes from an ore located in Khouribga (Morocco). A determined mass of the natural phosphate (125 μm) was transferred into a 500-mL conical flask; then, the dissolution reaction of the ore was carried out by adding a volume of 250 mL of the distilled water at 75 °C for 2 h. The precipitate was filtered under vacuum, washed with distilled water, and then dried in an oven at 100 °C. The dried phosphate was subjected to two treatments, firstly sodium hydroxide (1 M) and then with nitric acid (1 M) for 3 h. Filtered, washed, and dried, the solid was calcined at 900 °C.

2.2.3 Preparation of CS-Fa Composites

The cross-linked chitosan was prepared by dissolving 1 g of chitosan in 100 mL of 1% (v/v) acetic acid solution, and then a determined mass of Fa was added to the chitosan solution. The mixture is then stirred for 24 h. Finally, the resulting composite was washed with distilled water and dried at 50 °C overnight.

2.3 Characterizations

X-ray diffraction analysis was carried out using a Bruker D8 diffractometer operating at 45 kV/100 mA, using CuKα radiation with Ni filter. FTIR spectrometer was obtained using a thermo-scientific spectrometer in the mid-infrared region between 400 and 4000 cm^{-1} with a resolution of 4 cm^{-1}. The surface morphology of the samples was obtained from a scanning electron microscope (SEM) Philips XL 30 ESEM (Acc spot Magn 20.00 kV). Thermogravimetric analysis was performed using a Discovery TGA from TA instruments at a heating rate of 10 °C/min under nitrogen atmosphere.

2.4 Adsorption Studies

The adsorption experiments of Cr (VI) and CV onto CS and CS composite were carried out in a batch system. The adsorption tests were conducted in glass beakers (150 mL) containing 50 mL of CV/MB solutions at a consistent stirring rate. The effects of experimental parameters such as pH, adsorbent mass, contact time, initial chromium concentration, and temperature on the adsorption process were examined. The initial pH of the solution was adjusted by the addition of 0.1 M HCl or 0.1 M NaOH.

Table 1 CAS registry number and mass fraction purity

Component	CAS reg. no.	Supplies	Mass fraction
Potassium dichromate	7778-50-9	Sigma-Aldrich	≥ 0.995
Sodium hydroxide	1310-73-2	Sigma-Aldrich	≥ 0.98
1,5-Diphenylcarbazide	140-22-7	Sigma-Aldrich	≥ 0.98
Nitric acid	7697-37-2	Sigma-Aldrich	0.65
Hydrochloric acid	7647-01-0	Sigma-Aldrich	0.37
Sulfuric acid	7664-93-9	Sigma-Aldrich	0.37
Ethanol	64-17-5	Sigma-Aldrich	≥ 0.95

The concentration of Cr (VI) in the solution was determined using a UV-Vis spectrophotometer (UV-Vis 1200) at 540 nm. The adsorption capacity q_t (mg/g) and adsorption percentage (%Removal), at a specified contact time, were calculated using the following equations:

$$q_t = \frac{(C_o - C_t)V}{m} \quad (1)$$

$$\%\text{Removal} = \frac{(C_o - C_t)}{C_o} \times 100 \quad (2)$$

where C_o and C_t are the amounts of initial and retained Cr (VI) in the solution at time t (mg/L), respectively. V is the solution volume (L) and m is the mass of adsorbent (g).

2.5 Data Analysis

In order to describe the mechanism involved in the adsorption process, the experimental kinetic data were analyzed by application of the pseudo-first-order (PFO), the pseudo-second-order (PSO), and intraparticle diffusion (IPD) kinetic models, while Langmuir and Freundlich models were applied to describe the obtained isotherms to propose the sorption mechanism involved (Table 2) (Ho and Mckay 1998; Lagergren 1898; Langmuir 1916; U. 1906; Weber and Morris 1963). Thermodynamic parameters including the Gibbs free energy (ΔG), enthalpy (ΔH), and entropy (ΔS) were also analyzed to predict the feasibility and determine the nature of the adsorption process in the temperature range of 25–45 °C (Hameed et al. 2007; Tsai and Chang 1995).

2.6 Regeneration Study

The regeneration of the CS and CS-Fa was carried out using NaOH (0.5 N) solution as eluent for desorption of chromium ions (Cr (VI)). Desorption experiments were conducted by mixing 0.1 g of chromium loaded CS or CS-Fa with 50 mL of eluent at 25 °C for 2 h. The regenerated adsorbent was separated, then thoroughly washed with distilled water and then dried. The recovered materials were further subjected to adsorption experiments. This regeneration procedure was repeated up to six successive cycles. The loss of adsorbent mass after each regeneration cycle was considered to keep the same adsorbent/solution ratio in further use for adsorption.

Table 2 Kinetic and isotherm models

Model	Equation	Description
Kinetic models		
PFO	$\ln(q_e - q_e) = \ln q_e - k_1 t$	q_t (mg g^{-1}): the adsorbed amount of Cr(VI) at time t
PSO	$\frac{t}{q_t} = \frac{1}{k_2 q_e^2} + \frac{1}{q_e} t$	q_e (mg g^{-1}): the adsorbed amount of Cr(VI) at equilibrium k_1(min^{-1}), k_2 (g mg^{-1} min^{-1}) are: rate constants
IPD	$q_t = k_{int} t^{1/2} + C$	k_{int} (mg $min^{-½}$ g): intraparticular diffusion rate constant
Isotherm models		
Langmuir	$\frac{1}{q_e} = \frac{1}{q_m} + \frac{1}{q_m K_l C_e}$	q_e (mg g^{-1}): the adsorbed amount of Cr(VI) at equilibrium C_e (mg L^{-1}): concentration of Cr(VI) at equilibrium
Freundlich	$\ln q_e = \ln K_F + \frac{1}{n} \ln C_e$	K_L (L mg^{-1}): Langmuir constant; q_m: maximum adsorption capacity K_F (mg g^{-1}): equilibrium Freundlich constant n: adsorption intensity If $n > 1$, adsorption is favorable
Thermodynamic data		
Gibbs free energy	$\Delta G = -RT \ln k_d$	ΔG (kJ mol^{-1}): Gibbs free energy change; K_d: equilibrium constant; R: gas constant; T (°K): temperature
Van't Hoff	$\ln K_d = \frac{\Delta S^\circ}{R} - \frac{\Delta H^\circ}{RT}$	$\Delta S°$ (kJ mol^{-1}): entropy change; $\Delta H°$ (kJ mol^{-1}): enthalpy change R: gas constant (8.314 J mol^{-1} K^{-1})

3 Results and Discussion

3.1 Characterizations

3.1.1 X-ray Diffraction

X-ray patterns of CS, Fa, and CS-Fa composite were studied respectively in Fig. 1. The XRD pattern of biopolymer CS is depicted in Fig. 1. The diffractogram of prepared chitosan showed to 2θ, 10, and 20 corresponding the semi-crystalline patterns of chitosan (Sethy and Sahoo 2019), which has been confirmed by the JCPDS file no. 039-1894. Besides, Fig. 1 indicates the existence of a single fluorapatite phase with no characteristic peaks of impurities (e.g., CaO or tricalcium phosphate). As can be seen from Fig. 1, all diffraction peaks of Fa are in agreement with the standard pattern of fluorapatite (JCPDS file no.15-0876) with a hexagonal structure (Essamlali et al. 2019). The graphs of pure CS and Fa were taken as a reference to explain the data from the X-ray patterns of CS-Fa composite. The XRD patterns of CS-Fa is given in Fig. 3c showed impressive results since the major peaks and patterns in XRD data correspond to the composites. However, the characteristic peaks of Fa remain the same in the case of CS-Fa; a noticeable trend is that the peaks of CS become less defined, shifted in their initial position, and intensity also decreased. These results strongly show that the synthesis of CS-Fa composite was successfully realized under the chosen conditions.

3.1.2 FTIR Analysis

The characterization of chitosan by infrared spectroscopy is illustrated in Fig. 2; all bands that we found in this spectrum of chitosan are in good agreement with reported studies (Haffad et al. 2019; Song et al. 2013). The bands' attribution appearing in the spectrum are grouped in Table 3 (Nan et al. 2019).

The FTIR spectra of Fa impregnated in the CS biopolymer matrix confirm that some characteristic peaks of CS were shifted and others not. The broad peak between 3000 and 3600 cm^{-1} corresponding to the vibration of N–H and O–H changed its initial position and became more intense; the same remark was observed for the peak allocated to C–H symmetric stretching at 2930 cm^{-1}. The peak at 1661 cm^{-1} becomes very intense, while the peak at 800 cm^{-1} in the spectrum of Fa is almost disappearing, which confirms that residual *N*-acetyl (C=O stretching of amide I) reacted with the carbonate substitution of FA and formed a robust structure of CS-FA composite.

3.1.3 Scanning Electronic Microscopy-Energy-Dispersive X-ray Spectroscopy

The SEM image of obtained chitosan is presented in Fig. 3. Irregular structure and cracks can be clearly seen in SEM image of prepared CS. These characteristics (surface morphology with several cracks) give the sheet microstructure surface of CS. In total, surface changes were observed when CS-Fa was prepared. In fact, the surface becomes very rigorous and the particles of Fa

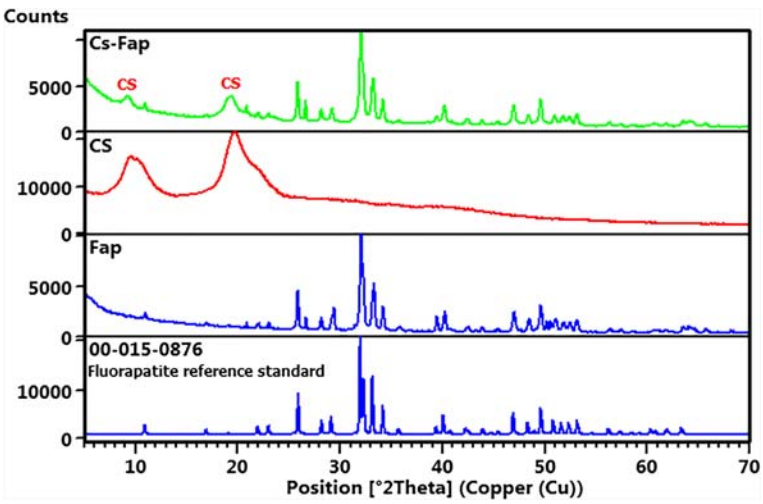

Fig. 1 X-ray patterns of chitosan (CS), fluorapatite (Fa), and CS-Fa composite

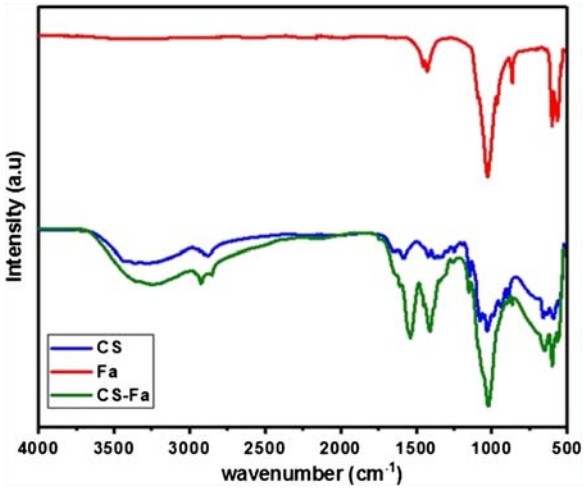

Fig. 2 FTIR spectra of chitosan (CS), fluorapatite (Fa), and CS-Fa composite

are well deposited on the sheet surface of CS in a fairly homogeneous way, which was confirmed by EDS analysis throughout the homogeneous distribution of Ca and P on CS-Fa.

3.1.4 Thermogravimetric Analysis

Next, the thermal stability of CS and CS-Fa was compared by TGA. According to Fig. 4, CS and CS-Fa showed a slight weight loss of 9% and 5%, respectively, at 100 °C that attributed to the evaporation of free water (non-bond) and hydrogen-bonded water (Abdel-Fattah et al. 2015; Dessì et al. 2013). More weight losses at 250 °C and 400 °C corresponded to the decomposition of volatile organic matter and released volatile substance of the thermal decomposition of the inorganic compound for CS and CS-Fa, respectively (Sivakumar et al. 2002). Additionally, it was observed that the CS decomposition was slowed when incorporated by FAP, suggesting good thermal stability to be applied as an adsorbent. The total weight losses were found to be 67% and 56% for CS and CS-Fa, respectively (Ali et al. 2018).

3.2 Adsorption Studies

3.2.1 The Effect of pH

The influence of pH on Cr (VI) adsorption onto CS and CS-Fa was studied in a pH range from 1.0 to 7.0, using 0.1 g of CS or CS-Fa in a 50 mL of Cr (VI) solution (10 mg/L) for 1 h at room temperature. The pH was adjusted using 0.1 mol/L NaOH and 0.1 mol/L HCl. The results are shown in Fig. 5a. At this pH range, the highest levels of Cr (VI) removal on CS (66.2%) and CS-Fa (92.0%) were observed at pH 3.0, and they dropped for CS to 19.8% and 21.22% at pH values of 1.0 and 7.0, respectively, while they decreased to 69.0% and 48.0% at pH values of 1.0 and 7.0, respectively for Cs-Fa. As shown in Fig. 5a, the Cr (VI) removal diminished as the solution pH increases from 3.0 to 7.0. Cr (VI) speciation in solution is recognized to be highly pH-dependent (Dinker and Kulkarni 2015). Chromic acid (H_2CrO_4) appears when the pH is less than 2.0. Also, when the pH ranged from 1.0 to the neutral pH 7.0, the $HCrO_4^-$ ions occur, while, above the neutral pH, only CrO_4^{2-} ions are present in the solution (Fig. S2) (Elouahli et al. 2018). As disclosed in Fig. 5a, the removal proficiency at lower pH values is higher because of the predominance of Cr (VI) species mainly exists in monovalent $HCrO_4^-$ form. As the pH increased, the CS and CS-Fa surface develops the negative

Table 3 FTIR bands' attribution of CS, Fa, and CS-Fa

Functional groups	Adsorption bands		
	CS	Fa	CS-Fa
N–H and O–H (vibration)	3000–3600 cm^{-1}	–	3000–3600 cm^{-1}
C–H (symmetric stretching)	2930 cm^{-1}	–	2922 cm^{-1}
C=O (stretching of amide I)	1661 cm^{-1}	–	1538 cm^{-1}
CH_2 (bending) CH_3 (symmetrical deformations)	1420 cm^{-1}	–	1421 cm^{-1}
C–O–C (asymmetric stretching)	1151 cm^{-1}	–	1148 cm^{-1}
C–O (stretching)	1030 cm^{-1}	–	1031 cm^{-1}
CO_3^{2-}	–	1460.5 and 875 cm^{-1}	1458 and 864 cm^{-1}
PO_4 (symmetric and asymmetric stretching υ3)	–	1043.8 cm^{-1} and 967.5 cm^{-1}	1031 cm^{-1} and 967.5 cm^{-1}
Bending vibrations of PO_4 tetrahedra υ4(PO4).	–	602.0 and 573.4 cm^{-1}	660 and 554 cm^{-1}

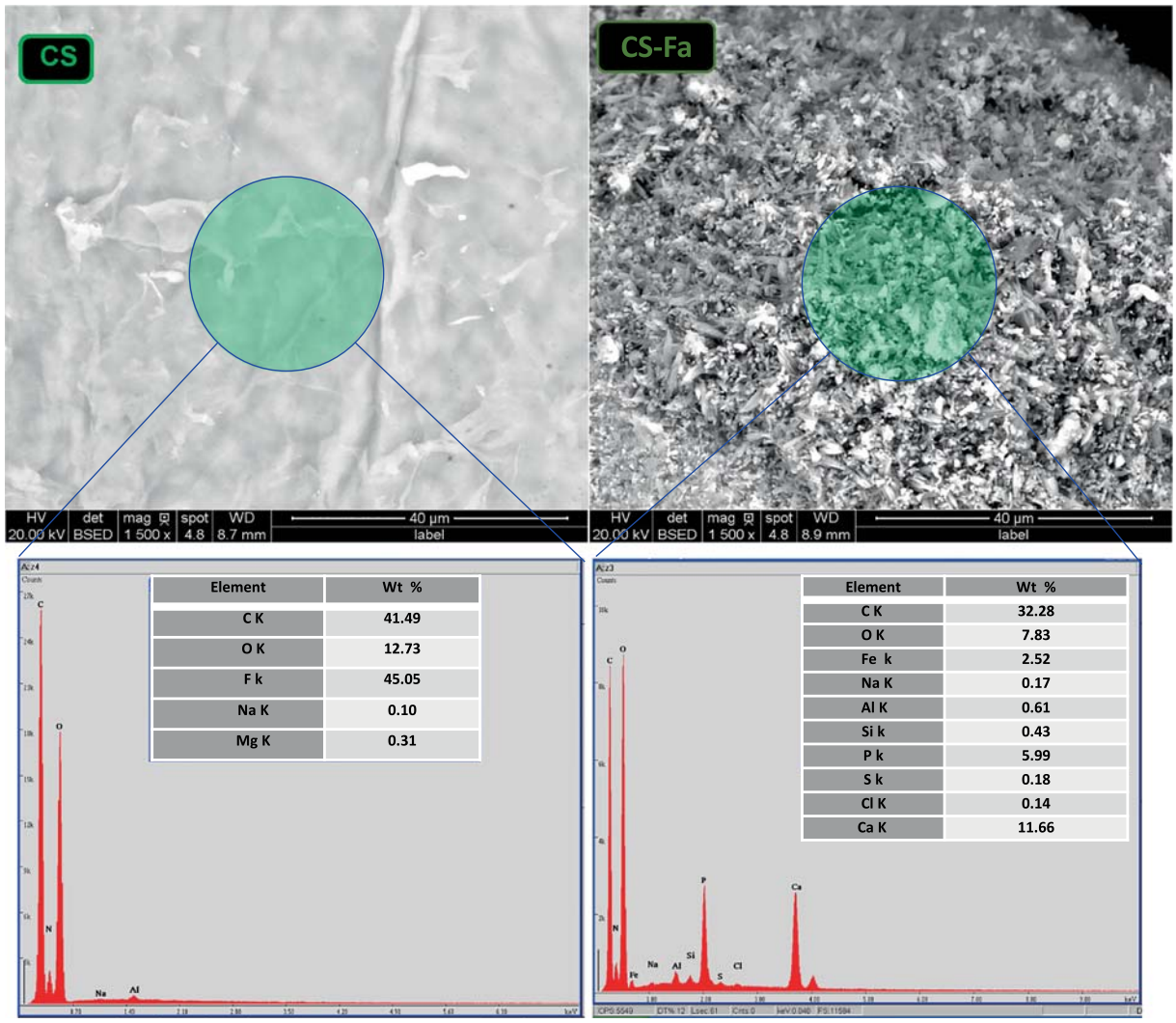

Fig. 3 SEM images and EDS analyses of chitosan (CS) and CS-Fa composite

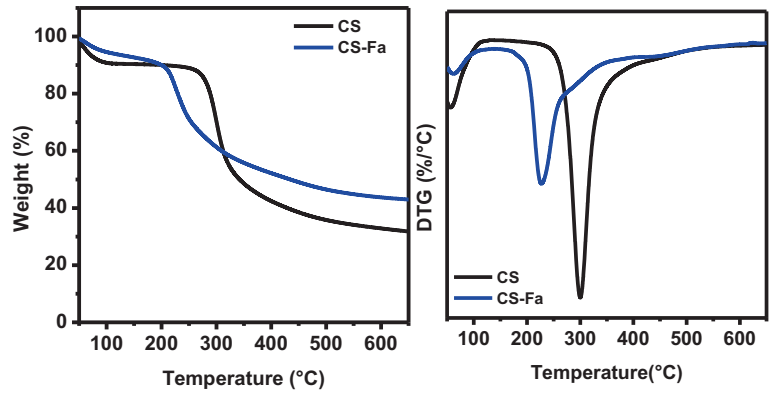

Fig. 4 TGA graphs of CS and CS-Fa

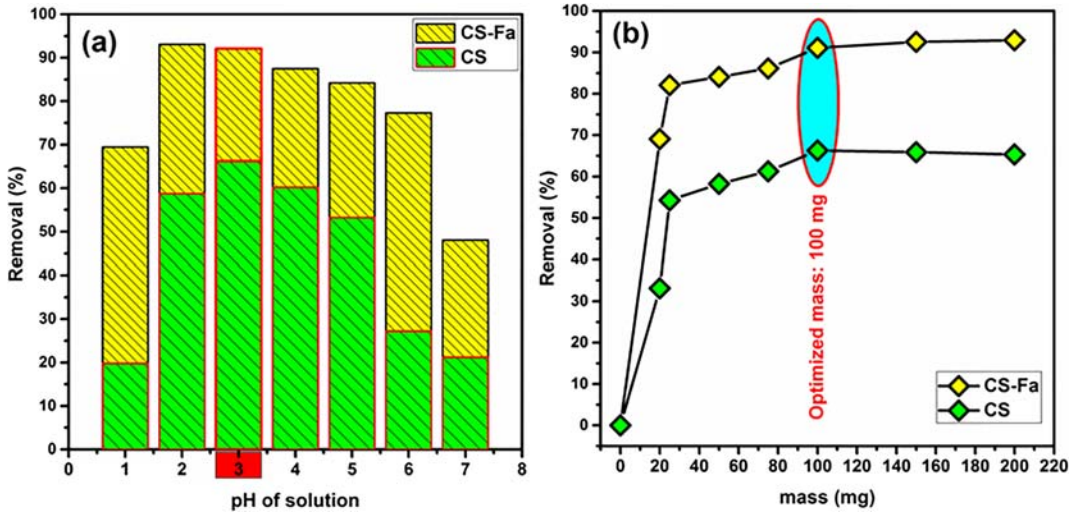

Fig. 5 **a** Effect of pH solution and **b** adsorbents mass on adsorption of Cr (VI)

surface charges increasingly, leading to a drop in the removal efficiency of Cr (VI). Consequently, the removal percentage of Cr (VI) at lower pH values ($pH < pH_{PZC}$) is higher compared to higher pH values (Fig. S1). This result demonstrates that the pH is a significant factor affecting the removal efficiency of Cr (VI) on CS and CS-Fa. Later studies of adsorption were carried out at pH 3.0.

3.2.2 The Effect of Adsorbent Mass

The effect of CS and CS-Fa dosage on Cr (VI) removal displayed in Fig. 5b shows that the percentage removal of Cr (VI) increases with increasing the amount of the adsorbent from 20 to 100 mg, and then it remains stable. This could be attributed to the availability of active binding sites (Abdellaoui et al. 2018). As Fig. 5b shows, 100 mg Cs-Fa was enough to remove over 91% of Cr (VI) (Ci = 100 mg/L), while 100 mg of Cs uptake was limited in 66.29%. In general, the removal of Cr (VI) by Cs-Fa was comparatively higher and faster than Cs materials, as will be discussed in the next section.

As the removal efficiency was to be the highest when we use 100 mg of CS and CS-Fa, it will be considered for further experiments.

3.2.3 Adsorption Kinetics

Figure 6 illustrates the adsorption of metal ions of Cr (VI) on CS and CS-Fa with different contact times (0 to 120 min). The adsorption capacity increase with

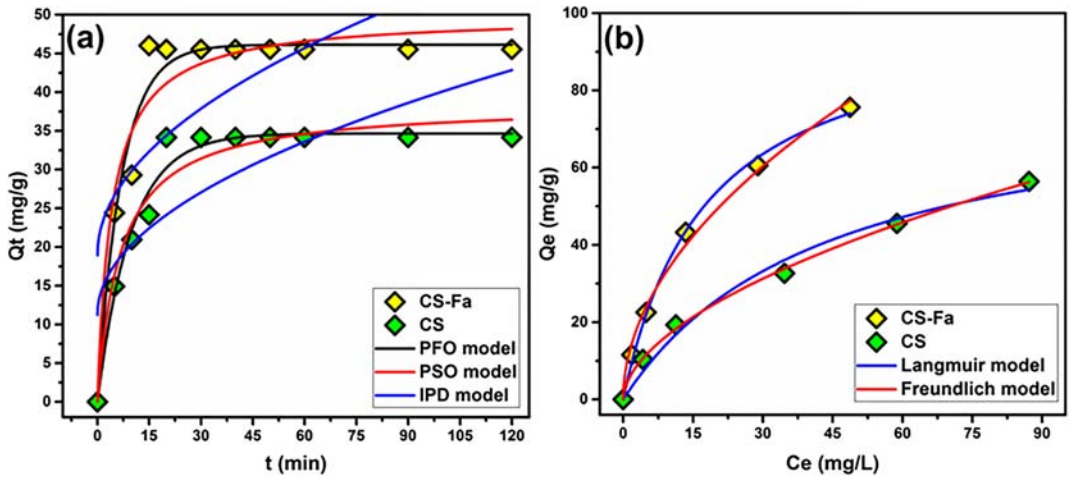

Fig. 6 **a** Kinetic studies by PFO, PSO, and IPD models. **b** Isotherm studies by Langmuir and Freundlich models

Table 4 Kinetics adsorption parameters of Cr(VI) on CS and CS-Fa

	Pseudo-first-order model				Pseudo-second-order model		
	$q_{e,exp}$ (mg/g)	$q_{e,cal}$ (mg/g)	K_1 (1/min)	R^2	$q_{e,cal}$ (mg/g)	K_2 (g/mg min)	R^2
CS	34.15	34.65	0.102	0.976	38.49	0.003	0.949
CS-Fa	45.53	46.12	0.142	0.968	49.84	0.004	0.941
Intraparticle diffusion model							
	K_{ip}			C		R^2	
CS	2.88			11.23		0.641	
CS-Fa	3.45			18.94		0.572	

increasing contact time up to 20 min and 15 min, respectively, for CS and CS-Fa, after which it is more constant. The higher adsorption of CS-Fa at the initial contact time compared to CS could be related to the driving force of Cr (VI) ions into the surfaces of CS-Fa and the abundance of active sites on the CS-Fa compared to CS (Li et al. 2010; Wu et al. 2008) (Table 4).

To examine the adsorption kinetics of Cr (VI) metal ion onto CS and CS-Fa and the mechanism and rate-controlling step in the whole adsorption process, the nonlinear forms of pseudo-first-order (PFO), pseudo-second-order (PSO), and intraparticle diffusion (IPD) models are used (Table 2). Table 2 summarizes the analogous parameters for Cr (VI) metal ion adsorption on CS and CS-Fa. The results showed that the R^2 of PSO and IPD exhibit a poor connection of Cr (VI) metal ion onto CS and CS-Fa as opposed to parameters of the PFO. In addition, PFO model show well-coordinating correlations between calculated Qcal values (CS 34.65 mg/g and CS-Fa 46.12 mg/g) and experimental q_e values (CS 34.15 mg/g and CS-Fa 45.53 mg/g).

3.2.4 Adsorption Isotherms

Langmuir and Freundlich isotherms (Table 2) were useful to define the adsorption capacity of CS and CS-Fa for Cr (VI) metal ion (Elouahli et al. 2018). The fitting plots of Langmuir and Freundlich isotherm models for Cr (VI) adsorption on CS and CS-Fa are shown in Fig. 6. The calculated isotherm parameters, along with correlation coefficients (R^2), are set in Table 5. Rendering to R^2 values ($R^2 > 0.997$), the Langmuir model tailored better than the Freundlich model to experimental data for the adsorption of Cr (VI) metal ion. Owing to the Langmuir model is established on the homogenous adsorption assumption, it can be said that the adsorption of Cr (VI) metal ion onto CS and CS-Fa surface is homogenous. By comparing the obtained q_{max}, the q_{max} values for CS-Fa (100.92 mg/g) is higher than CS (81.34 mg/g), which demonstrates the efficiency of the addition of Fa.

However, the higher sorption capacity of the CS-Fa composite compared to CS could be attributed to the presence of more reactive amino groups in chitosan as well as active binding sites already possess fluorapatite in the surface. Therefore, under the studied condition, the chromium fraction is negatively charged (mainly $HCrO_4^-$), which promotes strong electrostatic attraction with surface groups of CS-Fa (Kousalya et al. 2010). Consequently, it is confirmed that the use of composite possesses an enhanced sorption capacity, which demonstrates its selectivity towards Cr (VI) ions. Compared to some chitosan-based adsorbents reported in the literature, CS-Fa could be a promising and effective adsorbent for the removal of chromium ions from aqueous medium (Table 6).

Table 5 Equilibrium adsorption parameters of Cr(VI) on CS and CS-Fa

	Langmuir			Freundlich		
	q_{max} (mg/g)	K_L (L min^{-1})	R^2	K_F (mg/g)	n	R^2
CS	81.34	0.023	0.998	4.81	1.81	0.981
CS-Fa	100.92	0.056	0.997	10.58	1.95	0.992

Table 6 Adsorption capacity comparison of various chitosan-based adsorbents

Adsorbent	q_{max} (mg g^{-1})	Reference
Chitosan-g-PMMA	92.5	Sethy and Sahoo 2019
HDMTA-Zeolite-rich tuff	1.0	Salgado-gómez et al. 2014
Chitosan/graphene oxide/montmorillonite composite	87.03	Yu et al. 2017
Chitosan/montmorillonite	35.71	Chen et al. 2013
Cyclodextrin–chitosan/graphene oxide	67.66	Li et al. 2013
Chitosan-coated $MnFe_2O_4$	31.323	Xiao et al. 2013
Chitosan, GO/EDTA	86.17	Zhang et al. 2016
Cross-linked chitosan bentonite composite	89.13	Liu et al. 2015
CS-Fa	100.92	This study

3.2.5 Thermodynamic Study

One of the indispensable tools in the prediction of the adsorption mechanism, whether it is a physisorption or chemisorption process are the thermodynamic parameters. The thermodynamic parameters could be determined from the thermodynamic laws as it is presented in Table 1 (Fig. 7). The plots of thermodynamic parameters are listed in Table 7. The free energies of both adsorbents, CS and CS-Fa, exhibit negative values in the studied temperature range, indicating that the adsorptive of chromium has occurred favorably and spontaneously with low adsorption-energy requirements. The negative $\Delta H°$ quantities (− 32.549 and − 20.095 J/mol) suggest that the adsorption of Cr (VI) is exothermic onto CS and CS-Fa, respectively. Moreover, the decrease of ΔG values with increasing the temperature from 298 to 333 K asserted the exothermicity of the adsorption process, which was also confirmed by the negative value of ΔH. In addition, the $\Delta S° < 0$ reflects a decrease in the degree of freedom of Cr (VI) ions on the solid-solution interface of the adsorbents (Aydin and Aksoy 2009; Mobasherpour et al. 2011; Pal and Pal 2019).

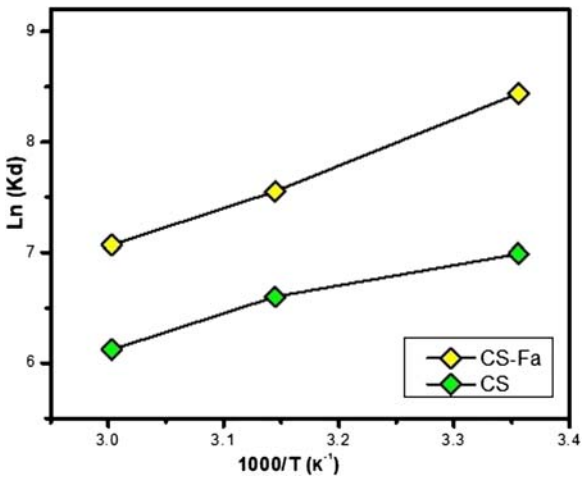

Fig. 7 Plot of ln(K_d) versus 1000/T for Cr(VI) adsorption onto CS and CS-Fa

3.3 Regeneration

The evaluation of the reusability and recovery of the adsorbents is one of the crucial factors in the adsorption processes. The CS and CS-Fa loaded Cr (VI) after adsorption were recovered using NaOH solution. From the results shown in Fig. 8 CS-Fa showed a high regeneration capacity compared to CS; however, the uptake ability of Cr (VI) using CS-Fa composite slightly decreased after four cycles from 89.32 to 79.7% in the sixth cycle. Whereas uptake percent was decreased from 66.8 in the initial three cycles to 52.5 in the fifth cycle. Accordingly, the synergistic use of the adsorbents (chitosan and fluorapatite) as a composite has improved the regeneration capacity of the adsorbent. Consequently, CS-Fa could be reused for the fifth time in the adsorption process of Cr (VI).

3.4 Modeling Using CCD-RSM

The adsorption of Cr onto CS and CS-Fa was optimized by using a multivariate analysis consisting of response surface methodology (RSM) coupled with central composite design (CCD) (Ait Ahsaine et al. 2017, 2018; Anfar et al. 2017). Therefore, the variables were assessed at five coded levels (− α, − 1, 0, + 1, and + α)

Table 7 Thermodynamic parameters of Cr(VI) using CS and CS-Fa

	$\Delta H°$ (KJ/mol)	$\Delta S°$ (J/mol K)	$\Delta G°$ (KJ/mol)		
			298 K	318 K	333 K
CS	− 32.549	− 39.217	− 17.317	− 17.455	− 16.943
CS-Fa	− 20.095	− 9.029	− 20.907	− 19.965	− 19.563

(Table S1). Appropriate parameters affecting the adsorption of Cr were found by using the data of the first step in this work. Therefore, pH, time, temperature, and mass were considered as the design variables. Ordinary equations and parameters of the second-order polynomial model have presented details elsewhere (Anfar et al. 2018; Zbair et al. 2018, 2019) (Table S1).

The obtained data were fed into a computer for statistical study. The results of statistical treatment are as follows:

- The relationship between the response (removal %) and variables was confirmed by ANOVA and shows a strong significance of variables at a 95% confidence level (P value < 0.05) for both cases (Cr adsorption onto CS and CS-Fa) (Anfar et al. 2018).
- Based on Table S2, the coefficients of determination values indicate a good fit between the experimental and calculated results by the model in the case of Cr adsorption onto CS-Fa and the opposite for Cr adsorption onto CS (Anfar et al. 2019b).
- The significance of the coefficients was examined using the P value (Table S2). Indeed, all coefficients are significant at 5% or 1% in both cases, except the pH effect, the interactions pH × temperature, temperature × time, and pH × mass (Anfar et al. 2019c).

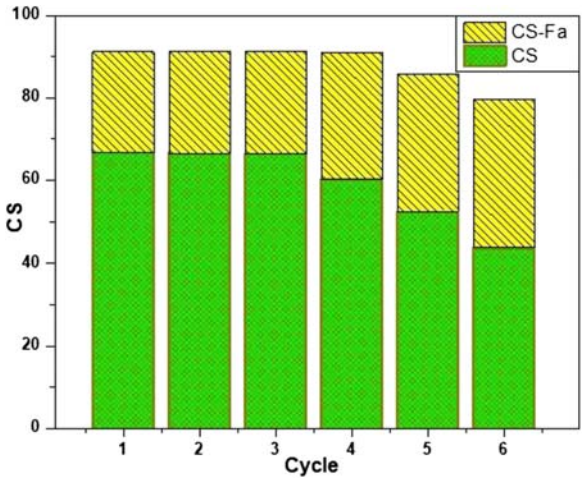

Fig. 8 Recycling study of CS and CS-Fa adsorbents

The results of CCD matrix were used to elaborate a quadratic polynomial equation for Cr adsorption onto CS-Fa (Eq. 1).

$$Adsorption\ (\%) = 88.033 + 0.265B + 2.398C + 1.141D - 2.014A^2 + 0.807B^2 CD - 1.396C^2 - 0.495D^2 - 1.193AC - 0.296BD - 1.247 \quad (1)$$

All reported considerable interactions among different parameters in the CCD were taking into account to determine most significant effects by using RSM presentations (Fig. S3) (Anfar et al. 2019a; Elouahli et al. 2018; Haffad et al. 2019; Ouasfi et al. 2019). Based on these three-dimensional response surface plots, the influence related to time and temperature depicted in Fig. S3-a indicates that high removal of Cr was found at this regain. The suggested optimized value by RSM for pH was found to be 2.54 for pH, 25.75 °C, 36.63 min, and by using of 86.72 mg of CS-Fa adsorbent. The estimated adsorption removal efficiency by the model, at these values, was 91.28%. Under some optimal conditions, the adsorption of Cr onto CS-Fa was carried out and led to an achievement of 91.8%. These results show an indication of proper accordance between estimated and experimental results and confirm the suitability of the model (Table S2).

4 Conclusion

In this study, it has been demonstrated that synergistic use of the adsorbents (chitosan and fluorapatite) as a composite has improved the sorption capacity of Cr (VI) and the regeneration capacity of the adsorbent as well. The chromium uptake was slightly influenced by the pH range from 2 to 6. The Langmuir isotherm model could be applied to the sorption of Cr (VI) ions, both sorbent CS and CS-Fa, with maximum capacities of 81.34 and

100.92 mg/g, respectively. The rate of sorption followed the pseudo-first-order kinetic model, where the process was spontaneous and exothermic in nature.

References

Abatal, M., Olguin, M. T., Abdellaoui, Y., & Bouari, A. E. L. (2018). Sorption of Cd (II), Ni (II) and Zn (II) on natural, sodium-, and acid-modified clinoptilolite-rich tuff. *Environment Protection Engineering, 44*(1), 42–59. https://doi.org/10.5277/epe180104.

Abdel-Fattah, W. I., Sallam, A. S. M., Diab, A. M., & Ali, G. W. (2015). Tailoring the properties and functions of phosphate/silk/Ag/chitosan scaffolds. *Materials Science and Engineering C, 54*, 158–168. https://doi.org/10.1016/j.msec.2015.05.015.

Abdellaoui, Y., Olguin, M. T., Abatal, M., Bassam, A., & Giácoman-Vallejos, G. (2019). Relationship between Si/Al ratio and the sorption of Cd (II) by natural and modified clinoptilolite-rich tuff with sulfuric acid. *Desalination and Water Treatment, 150*, 157–165. https://doi.org/10.5004/dwt.2019.23792.

Abdellaoui, Y., Olguín, M. T., Abatal, M., Ali, B., Díaz Méndez, S. E., & Santiago, A. A. (2018). Comparison of the divalent heavy metals (Pb, Cu and Cd) adsorption behavior by montmorillonite-KSF and their calcium- and sodium-forms. *Superlattices and Microstructures.* https://doi.org/10.1016/j.spmi.2017.11.061.

Ait Ahsaine, H., El Alem, N., Anfar, Z., Ezahri, M., & Zbair, M. (2017). Acridine orange adsorption by zinc oxide/almond shell activated carbon composite: operational factors, mechanism and performance optimization using central composite design and surface modeling. *Journal of Environmental Management, 206*, 383–397. https://doi.org/10.1016/j.jenvman.2017.10.058.

Ait Ahsaine, H., Zbair, M., Anfar, Z., Naciri, Y., El haouti, R., El Alem, N., & Ezahri, M. (2018). Cationic dyes adsorption onto high surface area 'almond shell' activated carbon: Kinetics, equilibrium isotherms and surface statistical modeling. *Materials Today Chemistry, 8*, 121–132. https://doi.org/10.1016/j.mtchem.2018.03.004.

Aklil, A., Mouflih, M., & Sebti, S. (2004). Removal of heavy metal ions from water by using calcined phosphate as a new adsorbent. *Journal of Hazardous Materials, 112*(3), 183–190. https://doi.org/10.1016/j.jhazmat.2004.05.018.

Ali, G. W., El-Hotaby, W., Hemdan, B., & Abdel-Fattah, W. I. (2018). Thermosensitive chitosan/phosphate hydrogel-composites fortified with Ag versus Ag@Pd for biomedical applications. *Life Sciences, 194*, 185–195. https://doi.org/10.1016/j.lfs.2017.12.021.

Anfar, Z., Ait Ahsaine, H., Zbair, M., Amedlous, A., Ait El Fakir, A., Jada, A., & El Alem, N. (2019a). Recent trends on numerical investigations of response surface methodology for pollutants adsorption onto activated carbon materials: A review. *Critical Reviews in Environmental Science and Technology*, 1–42. https://doi.org/10.1080/10643389.2019.1642835.

Anfar, Z., Amedlous, A., Ait El Fakir, A., Ait Ahsaine, H., Zbair, M., Lhanafi, S., El Haouti, R., Jada, A., & El Alem, N. (2019b). Combined methane energy recovery and toxic dye removal by porous carbon derived from anaerobically modified digestate. *ACS Omega, 4*(5), 9434–9445. https://doi.org/10.1021/acsomega.9b00524.

Anfar, Z., El Haouti, R., Lhanafi, S., Benafqir, M., Azougarh, Y., & El Alem, N. (2017). Treated digested residue during anaerobic co-digestion of Agri-food organic waste: methylene blue adsorption, mechanism and CCD-RSM design. *Journal of Environmental Chemical Engineering, 5*(6), 5857–5867. https://doi.org/10.1016/j.jece.2017.11.015.

Anfar, Z., Zbair, M., Ahsaine, H. A., Abdellaoui, Y., El Fakir, A. A., Amaterz, E. H., Jada, A., & El Alem, N. (2019c). Preparation and characterization of porous carbon@ZnO-NPs for organic compounds removal: classical adsorption versus ultrasound assisted adsorption. *ChemistrySelect, 4*(17), 4981–4994. https://doi.org/10.1002/slct.201901043.

Anfar, Z., Zbair, M., Ahsaine, H. A., Ezahri, M., & Alem, N. E. (2018). Well-designed WO3/activated carbon composite for rhodamine B removal: synthesis, characterization, and modeling using response surface methodology. *Fullerenes, Nanotubes, and Carbon Nanostructures, 26*(6), 389–397. https://doi.org/10.1080/1536383X.2018.1440386.

Aydin, Y. A., & Aksoy, N. D. (2009). Adsorption of chromium on chitosan: optimization, kinetics and thermodynamics. *Chemical Engineering Journal, 151*(1–3), 188–194. https://doi.org/10.1016/j.cej.2009.02.010.

Chen, D., Li, W., Wu, Y., Zhu, Q., Lu, Z., & Du, G. (2013). Preparation and characterization of chitosan/montmorillonite magnetic microspheres and its application for the removal of Cr (VI). 221, 8–15. https://doi.org/10.1016/j.cej.2013.01.089.

Cimá-Mukul, C. A., Abdellaoui, Y., Abatal, M., Vargas, J., Santiago, A. A., & Barrón-Zambrano, J. A. (2019). Eco-efficient biosorbent based on Leucaena leucocephala residues for the simultaneous removal of Pb (II) and Cd (II) ions from water system: sorption and mechanism. *Bioinorganic Chemistry and Applications, 2019*, 1–13. https://doi.org/10.1155/2019/2814047.

Dessì, M., Borzacchiello, A., Mohamed, T. H. A., Abdel-Fattah, W. I., & Ambrosio, L. (2013). Novel biomimetic thermosensitive β-tricalcium phosphate/chitosan-based hydrogels for bone tissue engineering. *Journal of Biomedical Materials Research - Part A, 101*(10), 2984–2993. https://doi.org/10.1002/jbm.a.34592.

Dinker, M. K., & Kulkarni, P. S. (2015). Recent advances in silica-based materials for the removal of hexavalent chromium: a review. *Journal of Chemical and Engineering Data, 60*(9), 2521–2540. https://doi.org/10.1021/acs.jced.5b00292.

Elouahli, A., Zbair, M., Anfar, Z., Ahsaine, H. A., Khallok, H., Chourak, R., & Hatim, Z. (2018). Apatitic tricalcium phosphate powder: high sorption capacity of hexavalent chromium removal. *Surfaces and Interfaces, 13*, 139–147. https://doi.org/10.1016/j.surfin.2018.09.006.

Essamlali, Y., Amadine, O., Fihri, A., & Zahouily, M. (2019). Sodium modified fluorapatite as a sustainable solid bi-functional catalyst for biodiesel production from rapeseed

oil. *Renewable Energy, 133*, 1295–1307. https://doi.org/10.1016/j.renene.2018.08.103.

Haffad, H., Zbair, M., Anfar, Z., Ahsaine, H. A., Bouhlal, H., & Khallok, H. (2019). Removal of reactive red-198 dye using chitosan as an adsorbent: optimization by central composite design coupled with response surface methodology. Toxin Reviews, *0*(0), 1–13. https://doi.org/10.1080/15569543.2019.1584822.

Hameed, B. H., Ahmad, A. A., & Aziz, N. (2007). Isotherms, kinetics and thermodynamics of acid dye adsorption on activated palm ash. *Chemical Engineering Journal, 133*(1–3), 195–203. https://doi.org/10.1016/j.cej.2007.01.032.

Ho, Y. S., & Mckay, G. (1998). Kinetic models for the sorption of dye from aqueous solution by wood. *In Trans IChemE, 76*.

Huang, R., Yang, B., & Liu, Q. (2013). Removal of chromium (VI) ions from aqueous solutions with protonated crosslinked chitosan. *Journal of Applied Polymer Science, 129*(2), 908–915. https://doi.org/10.1002/app.38685.

Hughes, J. M., & Rakovan, J. (2002). The Crystal structure of apatite, Ca5(PO4)3(F,OH,Cl). Reviews in Mineralogy and Geochemistry, 48(1), 1–12. https://doi.org/10.2138/rmg.2002.48.1.

Kousalya, G. N., Rajiv Gandhi, M., & Meenakshi, S. (2010). Removal of toxic Cr (VI) ions from aqueous solution using nano-hydroxyapatite-based chitin and chitosan hybrid composites. *Adsorption Science and Technology, 28*(1), 49–64. https://doi.org/10.1260/0263-6174.28.1.49.

Lagergren, S. (1898). Zur theorie der sogenannten adsorption geloster stoffe. In *Kungliga Svenska Vetenskapsakademiens* (Handlingar, Vol. 24).

Langmuir, I. (1916). The constitution and fundamental properties of solids and liquids. *Part I. Solids. Journal of the American Chemical Society, 38*(11), 2221–2295. https://doi.org/10.1021/ja02268a002.

Li, L., Fan, L., Sun, M., Qiu, H., Li, X., Duan, H., & Luo, C. (2013). Adsorbent for hydroquinone removal based on graphene oxide functionalized with magnetic cyclodextrin-chitosan. *International Journal of Biological Macromolecules, 58*, 169–175. https://doi.org/10.1016/j.ijbiomac.2013.03.058.

Li, Y., Du, Q., Wang, X., Zhang, P., Wang, D., Wang, Z., & Xia, Y. (2010). Removal of lead from aqueous solution by activated carbon prepared from Enteromorpha prolifera by zinc chloride activation. *Journal of Hazardous Materials, 183*(1–3), 583–589. https://doi.org/10.1016/j.jhazmat.2010.07.063.

Liu, Q., Yang, B., Zhang, L., & Huang, R. (2015). Adsorptive removal of Cr (VI) from aqueous solutions by cross-linked chitosan/bentonite composite. *Korean Journal of Chemical Engineering, 32*(7), 1314–1322. https://doi.org/10.1007/s11814-014-0339-1.

Mobasherpour, I., Salahi, E., & Pazouki, M. (2011). Removal of nickel (II) from aqueous solutions by using nano-crystalline calcium hydroxyapatite. *Journal of Saudi Chemical Society, 15*(2), 105–112. https://doi.org/10.1016/j.jscs.2010.06.003.

Nan, N., Zhu, Y., & Han, Y. (2019). Flotation performance and mechanism of α-Bromolauric acid on separation of hematite and fluorapatite. *Minerals Engineering, 132*(September 2018), 162–168. https://doi.org/10.1016/j.mineng.2018.11.048.

Ouasfi, N., Zbair, M., Bouzikri, S., Anfar, Z., Bensitel, M., Ait Ahsaine, H., Sabbar, E., & Khamliche, L. (2019). Selected pharmaceuticals removal using algae derived porous carbon: experimental, modeling and DFT theoretical insights. *RSC Advances, 9*(17), 9792–9808. https://doi.org/10.1039/C9RA01086F.

Pal, P., & Pal, A. (2019). Treatment of real wastewater: kinetic and thermodynamic aspects of cadmium adsorption onto surfactant-modified chitosan beads. *International Journal of Biological Macromolecules, 131*, 1092–1100. https://doi.org/10.1016/j.ijbiomac.2019.03.121.

Panda, L., Das, B., & Rao, D. S. (2011). Studies on removal of lead ions from aqueous solutions using iron ore slimes as adsorbent. *Korean Journal of Chemical Engineering, 28*(10), 2024–2032. https://doi.org/10.1007/s11814-011-0094-5.

Rojas, G., Silva, J., Flores, J. A., Rodriguez, A., Ly, M., & Maldonado, H. (2005). Adsorption of chromium onto cross-linked chitosan. *Separation and Purification Technology, 44*(1), 31–36. https://doi.org/10.1016/j.seppur.2004.11.013.

Salgado-gómez, N., Macedo-miranda, M. G., & Olguín, M. T. (2014). Chromium VI adsorption from sodium chromate and potassium dichromate aqueous systems by hexadecyltrimethylammonium-modified zeolite-rich tuff. *Applied Clay Science*. https://doi.org/10.1016/j.clay.2014.04.013.

de Sampaio, C., G., Frota, L. S., Magalhães, H. S., Dutra, L. M. U., Queiroz, D. C., Araújo, R. S., Becker, H., de Souza, J. R. R., Ricardo, N. M. P. S., & Trevisan, M. T. S. (2015). Chitosan/mangiferin particles for Cr (VI) reduction and removal. *International Journal of Biological Macromolecules, 78*, 273–279. https://doi.org/10.1016/j.ijbiomac.2015.03.038.

Sessarego, S., Rodrigues, S. C. G., Xiao, Y., Lu, Q., & Hill, J. M. (2019). Phosphonium-enhanced chitosan for Cr (VI) adsorption in wastewater treatment. *Carbohydrate Polymers, 211*(Vi), 249–256. https://doi.org/10.1016/j.carbpol.2019.02.003.

Sethy, T. R., & Sahoo, P. K. (2019). Highly toxic Cr (VI) adsorption by (chitosan-g-PMMA)/silica bionanocomposite prepared via emulsifier-free emulsion polymerisation. *International Journal of Biological Macromolecules, 122*, 1184–1190. https://doi.org/10.1016/j.ijbiomac.2018.09.069.

Sivakumar, M., Manjubala, I., & Panduranga Rao, K. (2002). Preparation, characterization and in-vitro release of gentamicin from coralline hydroxyapatite-chitosan composite microspheres. *Carbohydrate Polymers, 49*(3), 281–288. https://doi.org/10.1016/S0144-8617(01)00331-9.

Song, C., Yu, H., Zhang, M., Yang, Y., & Zhang, G. (2013). Physicochemical properties and antioxidant activity of chitosan from the blowfly Chrysomya megacephala larvae. *International Journal of Biological Macromolecules, 60*, 347–354. https://doi.org/10.1016/j.ijbiomac.2013.05.039.

Streimikiene, D. (2015). Environmental indicators for the assessment of quality of life. *Intellectual Economics, 9*(1), 67–79. https://doi.org/10.1016/j.intele.2015.10.001.

Sun, Z., Chen, D., Chen, B., Kong, L., & Su, M. (2018). Enhanced uranium (VI) adsorption by chitosan modified phosphate rock. Colloids and Surfaces A: Physicochemical and Engineering Aspects, 547(February), 141–147. https://doi.org/10.1016/j.colsurfa.2018.02.043.

Tsai, W. T., & Chang, C. Y. (1995). Surface characterization and thermodynamics of adsorption of methylene chloride on activated carbons. *Journal of Environmental Science and*

Health. Part A: Environmental Science and Engineering and Toxicology, 30(3), 525–535. https://doi.org/10.1080/10934529509376215.

U., F (1906). Die adsorption in lusungen (Vol. 57, Issue 0, pp. 385–470). Journal of Physical Chemistry.

Uddin, M. K. (2017). A review on the adsorption of heavy metals by clay minerals, with special focus on the past decade. *Chemical Engineering Journal, 308*, 438–462. https://doi.org/10.1016/j.cej.2016.09.029.

Weber, W. J., & Morris, J. C. (1963). Kinetics of adsorption on carbon from solutions. *Journal of the Sanitary Engineering Division, 89*, 31–60.

Wu, Y., Zhang, S., Guo, X., & Huang, H. (2008). Adsorption of chromium (III) on lignin. *Bioresource Technology, 99*(16), 7709–7715. https://doi.org/10.1016/j.biortech.2008.01.069.

Xiao, Y., Liang, H., Chen, W., & Wang, Z. (2013). Applied surface science synthesis and adsorption behavior of chitosan-coated MnFe 2 O 4 nanoparticles for trace heavy metal ions removal. *Applied Surface Science, 285*, 498–504. https://doi.org/10.1016/j.apsusc.2013.08.083.

Yu, P., Wang, H., Bao, R., Liu, Z., Yang, W., Xie, B., & Yang, M. (2017). Self-assembled sponge-like chitosan/reduced graphene oxide/montmorillonite composite hydrogels without cross-linking of chitosan for effective Cr (VI) sorption. *Vi*. https://doi.org/10.1021/acssuschemeng.6b02254.

Zbair, M., Ahsaine, H. A., Anfar, Z., & Slassi, A. (2019). Carbon microspheres derived from walnut shell: rapid and remarkable uptake of heavy metal ions, molecular computational study and surface modeling. *Chemosphere, 231*, 140–150. https://doi.org/10.1016/j.chemosphere.2019.05.120.

Zbair, M., Ait Ahsaine, H., & Anfar, Z. (2018). Porous carbon by microwave assisted pyrolysis: an effective and low-cost adsorbent for sulfamethoxazole adsorption and optimization using response surface methodology. *Journal of Cleaner Production*. https://doi.org/10.1016/j.jclepro.2018.08.155.

Zhang, L., Luo, H., Liu, P., Fang, W., & Geng, J. (2016). A novel modified graphene oxide/chitosan composite used as an adsorbent for Cr (VI) in aqueous solutions. *International Journal of Biological Macromolecules, 87*, 586–596. https://doi.org/10.1016/j.ijbiomac.2016.03.027.